Chapter 6
Results

The following chapter presents experimental work relating to various parts of the apparatus. The noise floor of the detection system is particularly dependent on a stable and reliable continuous-culture system. Results are presented from this along with those relating to the mm-wave characteristics of the exposure cell and the analysis system. These are necessary for the validation of the screening system.

6.1 Continuous culture system

The performance of the continuous-culture system was tested under a variety of conditions and with different strains of photobacteria. Initial experimentation concentrated on establishing the simplest configuration that would allow long-term maintenance of both growth and luminosity. As the response of the culture to fresh medium was complex (see Chapter 4) it was necessary perform a number of experiments that involved the addition of fresh medium to a steady-state system. Experiments were then performed with the system running on a single control variable i.e. luminosity or turbidity. The control system comprised two proportional-integral-derivative (PID) controllers, the optimal tuning parameters being established empirically.

6.1.1 Response to introduction of fresh medium

Fig. 15 illustrates (*Vibrio fischeri* NRRL-11177) the response of the culture absorbance and bioluminescence (emission) to the introduction of fresh medium. At point A medium flow was initiated at a rate of 15 ml hr^{-1}, then stopped at point B after continuation for 10 min. This dilution rate is much greater than the growth rate of the organism and would eventually cause the reaction vessel to “wash-out”. Emission was inhibited by the introduction of fresh medium and absorbance decreased in manner consistent with the volume of the reaction vessel and the growth rate of

the organisms over the time interval between point A and point B. After cessation of the medium-flow, emission rapidly recovered point C and exceeded the initial steady-state level. The absorbance also recovered in a manner that was predictable in terms of established models for bacterial growth. The graph clearly shows that bioluminescence and growth are not tightly coupled. In later studies, signal averaging was used to minimise fluctuations in bioluminescence due to stirrer bar rotation and air supply.

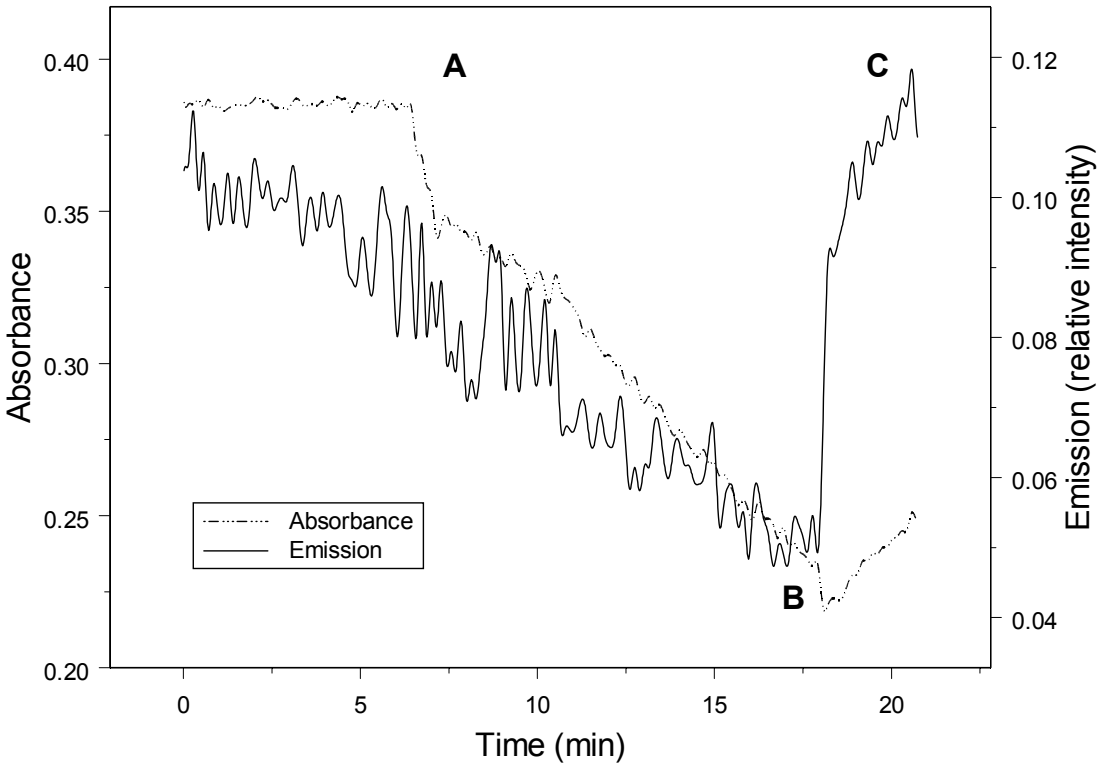

FIG. 15. Response of bioluminescence with the introduction of fresh medium A: Flow initiated. B: Flow stopped C: Recovery of bioluminescence

6.1.1 Operating the culture device as a turbidostat

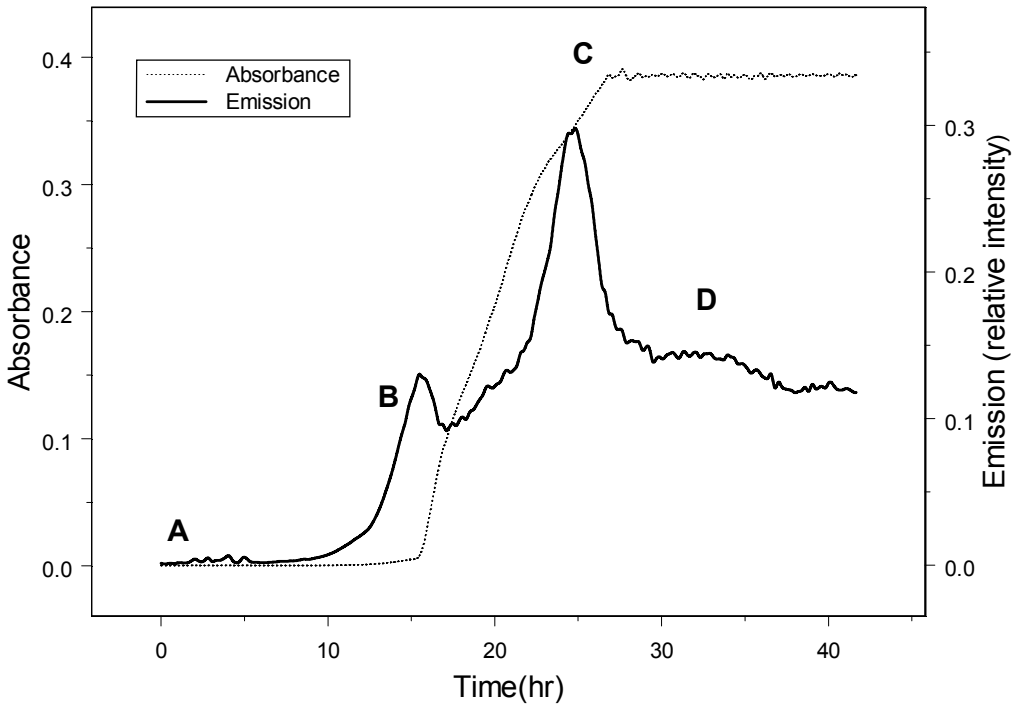

FIG. 16. A: Inoculation of reaction vessel with luminous culture B: Growth and bioluminescence in the reaction vessel are not tightly coupled C: Turbidity-controlled growth initiated with PID tuned so that medium flow is frequently initiated D: Loss of bioluminescence under this regime.

As described in chapter 4, the continuous culture system can be operated as a turbidostat. In the diagram above (Fig. 16) the reaction vessel was inoculated at point A with 0.1 ml of brightly luminous culture. The culture was grown at 298 K using the method described in detail in Chapter 4. Bioluminescence was initially detected between 10 and 15 hr after inoculation although this varied between different runs. Significant fluctuations in bioluminescence occurred that were not coupled to growth. After approximately 15 hr a detectable change in light transmission through the reaction vessel using the LED / photodiode pair described in chapter 4 was measured.

The growth rate of the culture appears to decrease slightly towards point C and this may be related to a higher density culture and entry into the stationary phase. At point C medium flow was initiated in response to changes in turbidity. A proportional-control (PID) algorithm was used to control turbidity to within ± 1% of the set point over an extended period. On using this regime it was possible to control cell density although this did not result in the required stable bioluminescence for use in the high-throughput analysis system. However, luminescence in the turbidostat was inconsistent and light intensity fell over a period of several hours.

6.1.2 Optimized long-term maintenance of photobacterium

Fig. 17 illustrates three graphs with the same time axis taken directly from the Labview control panel. The upper graph relates to emission, the middle graph turbidity and the lower graph, to the activity of the medium feed pump. The dual set-point system was deployed so that medium flow could be initiated by change in either turbidity or emission.

The tuning parameters were adjusting empirically and bioluminescence could be maintained within ± 10 % of the set point value (see upper window fig. 17). The tuning parameters for turbidity were intentionally set so that medium flow occurred intermittently. In this case inhibitory effect of fresh medium on emission could be minimized and it could therefore be used as a control parameter. The most successful long-term control strategy was not based on tightly coupling the PID controllers to input variables but rather using a highly damped response combined with high medium flow rate (15 ml hr^{-1}) to the bioreactor. Unlike a chemostat the turbidostat and bioluminostat use a closed loop control methodology and this is associated with intermittent flow. The tuning parameters for the turbidity PID controller: - P = 0.001, I = 25, D = 10.

The relative weighting of luminescence and turbidity as control components were selected and optimized. During combined control, the mean medium flow rate was approximately 3.7 ml h^{-1} (dilution rate

0.18 h^{-1}) for NRRL B-1117 with the transfer pump operating at a maximum of 1 ml h^{-1}.

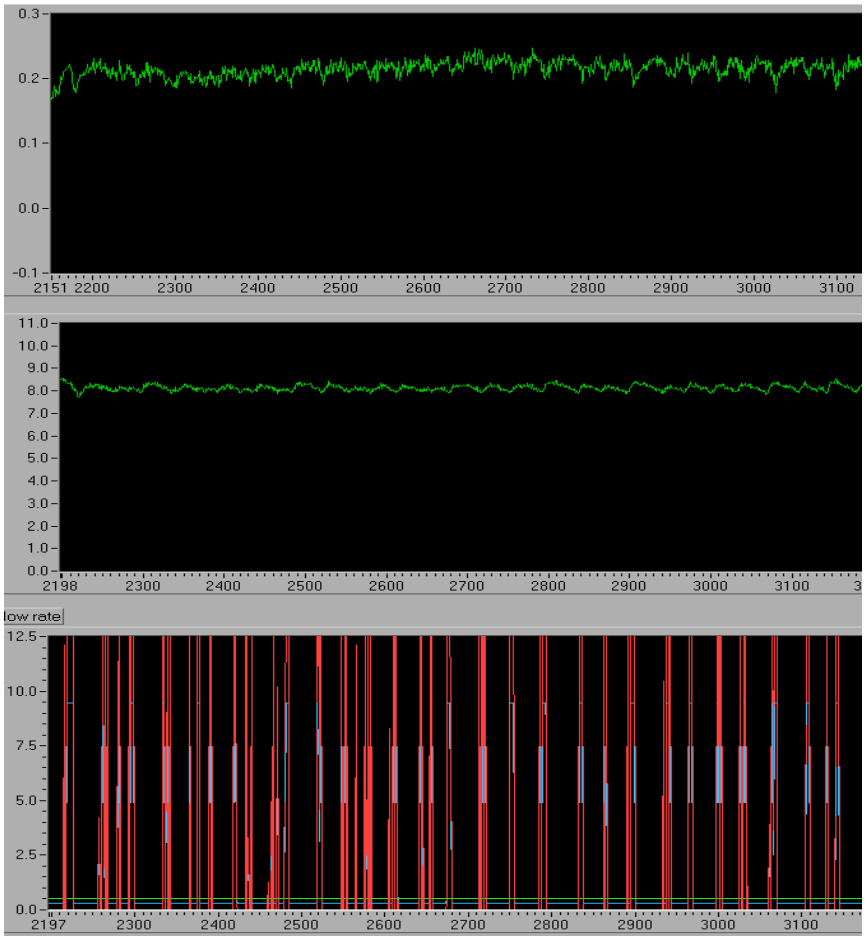

FIG. 17. Taken directly from the Labview control panel, continuous-culture device activity over a 25 h period using the regime described in the text. Top window: emission middle window: absorbance and lower window pump activity.

6.1.3 Oxygen

Oxygen is an essential co-factor in the production of light in marine bioluminescent bacteria. The miniaturized continuous culture system omitted an oxygen sensor normally found in larger-scale culture fermentation systems. A sharp decrease in emission could be obtained by disconnecting the oxygen supply to the sparge tube. This was measured quantitatively and features such as the residual bioluminescence and “excess flash” phenomena upon restoration of

oxygen supply were observed. Owing to the aerobic metabolic activity of the culture, oxygen tension falls to a very low level in approximately 5 min.

6.1.4 Effect of chemical toxicants of photobacterium

A positive control was required to validate the analysis system. An indication of the potential sensitivity could also be determined of the biosensor. In this study some effectors of energy metabolism were tested the most potent being venturicidin, where a concentration of 10^{-14} mol^{-1} L^{-1} resulted in a 50% inhibition in bioluminescence (see appendix D).

6.2 Calibration and measurement of the millimetre-wave exposure cell

As described in chapter 5, cultured organisms from the segmented flow system are exposed in a fundamental-mode waveguide exposure cell that is intersected by a sample tube. Simulation and measurements of this exposure cell using a vector network analyser were (VNA) (8510c, Hewlett Packard, Palo Alto, Ca, USA) made to establish with a high degree of confidence the energy absorbed by each sample segment. The cell operates in the fundamental mode over the 26 – 40 GHz range although measurements with the network analyser revealed values slightly outside this range (24 – 42 GHz) A response calibration was performed on the symmetrical limb test set-up (see Chapter 5) The insertion loss of the empty exposure cell was also measured and found to be negligible. The insertion loss of an empty cuvette (PTFE) is very small in comparison with a loaded 1 mm bore cuvette (PTFE) as shown on Fig. 18. This accounts for the large temporal variation of the transmission characteristic S_{21} with segmented flow.

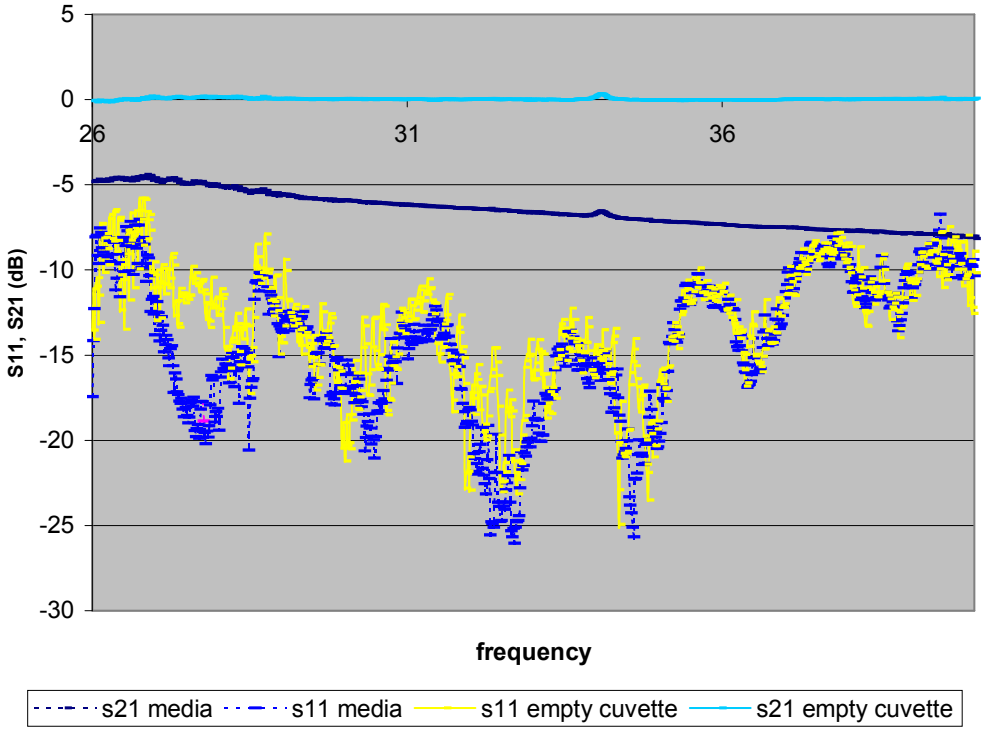

Fig. 18 The return and transmission losses of an empty and loaded cuvette

6.2.1 Return and transmission losses of different tubing materials

It is important to minimize losses in the tubing material. In particular the chemical characteristics of the tube were selected so that no frequency-specific absorption effects coincided with the frequency range under study. An equally important issue related to frequency-specific reflection form the tube material. Candidate tubing materials were initially selected for their dielectric characteristics and then measurements were made with the VNA over the operational range of the cell. Return and transmission losses of quartz tubing, two types of silicon tubing and PTFE tubing were measured.

6.2.2 Return and transmission losses of different sample materials

The VNA was used to measure transmission and absorption losses in the tube and a range of sample materials. A number of reference materials with known dielectric properties were characterized. Pure water and saline 4 % were compared against a synthetic seawater-peptone medium used for growing Photobacterium. The addition of peptone and yeast extract was not found to significantly change the dielectric properties compared with 4 % saline (see Fig, 19.).

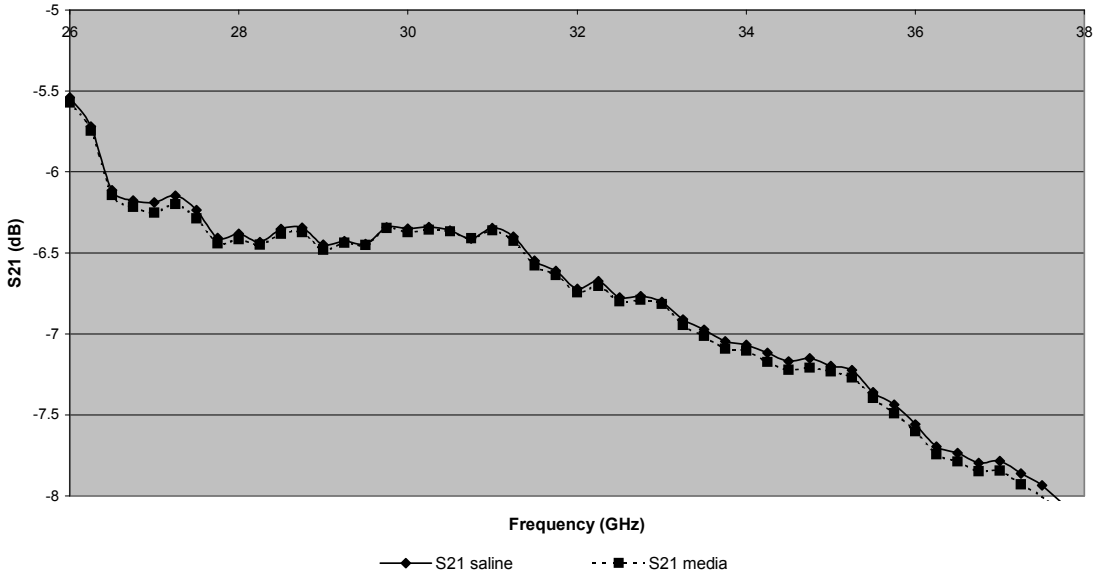

Fig. 19. Cuvette loaded with saline and Photobacterium growth media.

6.2.3 Transmission losses of different tubing bore

As expected increasing the internal bore of the cuvette increases transmission loss (S_{21}). In Fig. 20 the difference between a 0.5 mm and 1 mm internal bore cuvette (both filled with media) is shown.

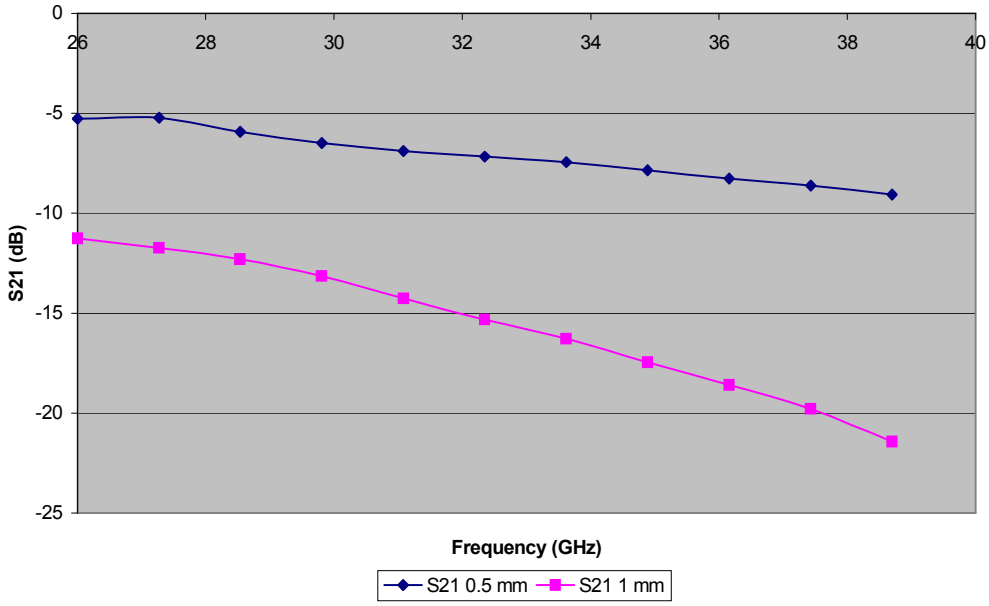

Fig. 20. Effect of increasing internal bore on transmission loss (S_{21}).

6.3 Simulation results

A representation of the fundamental mode exposure cell was created using Ansoft high frequency structure simulator (HFSS) (Ansoft corp. USA) based on a finite-element method solver. Dielectric data for the different materials was taken from a variety of sources. For some of the materials values were given in the simulator itself. Stogryn's equations for calculating the dielectric constant of saline water were used to create a lookup table over the operational frequency range of the cell for 4 % saline. Fig. 22 shows the simulated electrical field distribution in the tube sample at 27.5 GHz.

The simulation is highly dependent on the accurate representation of the dielectric properties of the biological culture medium. The laboratory temperature was maintained at 298 K ±1 K throughout the experiment. The returned (S_{11}) and transmitted (S_{21}) powers were measured at 51 equally spaced points between 27.5 and 35 GHz using VNA and compared with result derived from simulation.

In addition, simulated S_{11} and S_{21} parameters were generated for the 27.5 – 35.0 GHz frequency range at 51 points. Also shown is evanescent mode propagation at the points where the tube intersects the waveguide wall, which may be used to estimate the isolation between the exposure cell and pre-exposure detector.

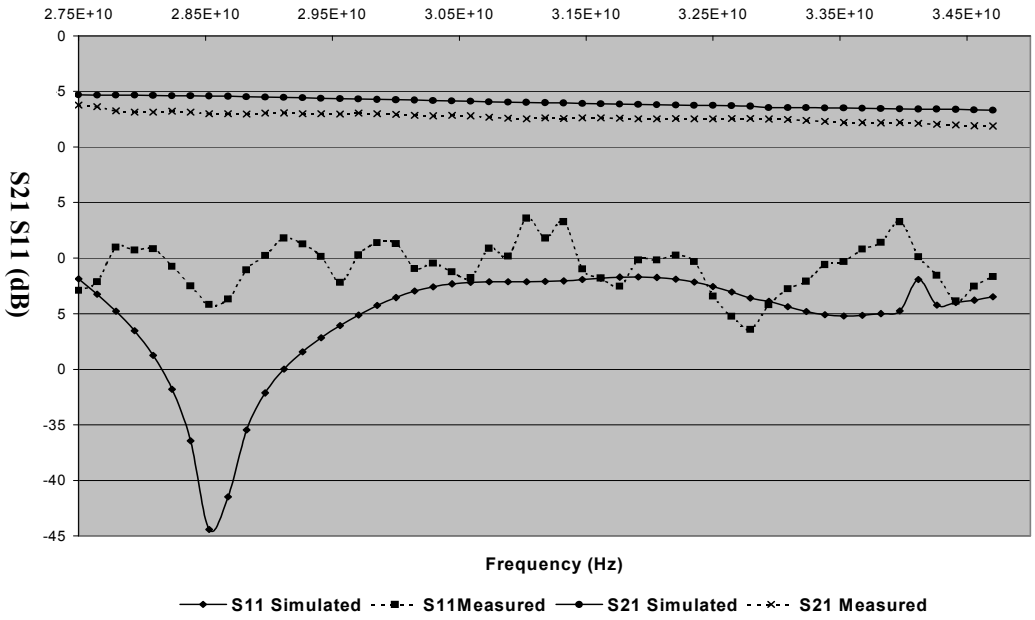

Fig. 21 Simulated and measured S_{11} and S_{21} Parameters

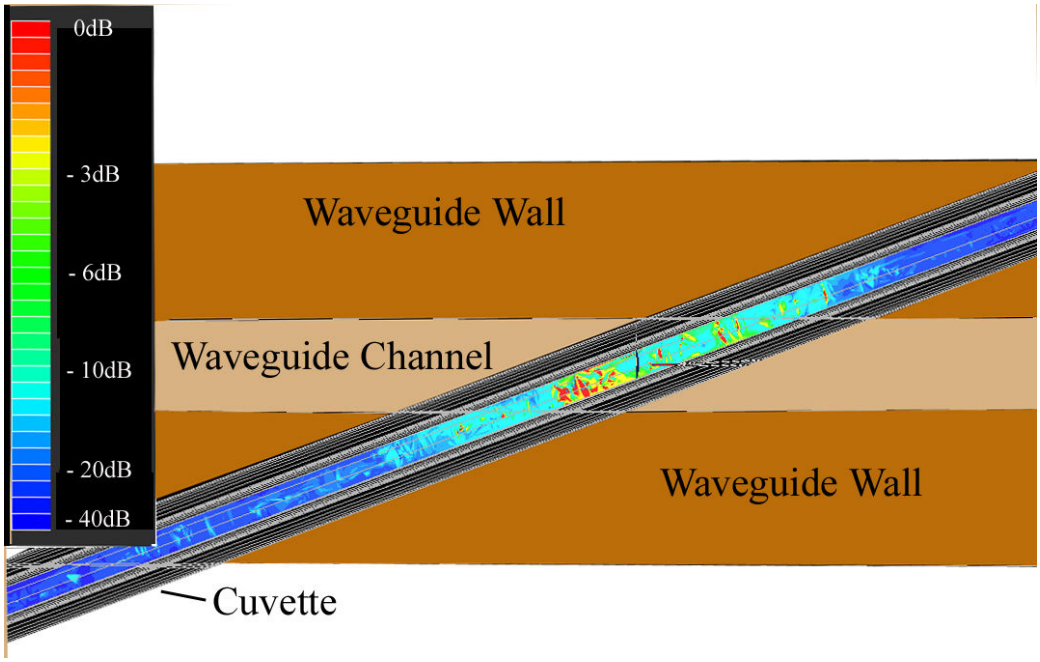

Fig. 22. Electric field distribution with a 4 % saline sample in the tube

The simulated S_{11} and S_{21} show good general agreement. Certain deviations do occur however. Transmission loss, S_{21} is subject to a systematic deviation of approximately 2 dB with the simulation data giving slightly higher attenuation. The reflected power was small in comparison with that transmitted which could be accounted for with the low insertion angle of the tube. A dip in reflected power was measured with the simulation but not the VNA. The simulation and measurement data were used to calculate sample SAR for a levelled 1 mW source power. Sweeping across the frequency band resulted in small variations in average SAR, which amounted to (± 10 %) of the target SAR. In Fig. 20 slight asymmetry of the model occurred at different spot frequencies.

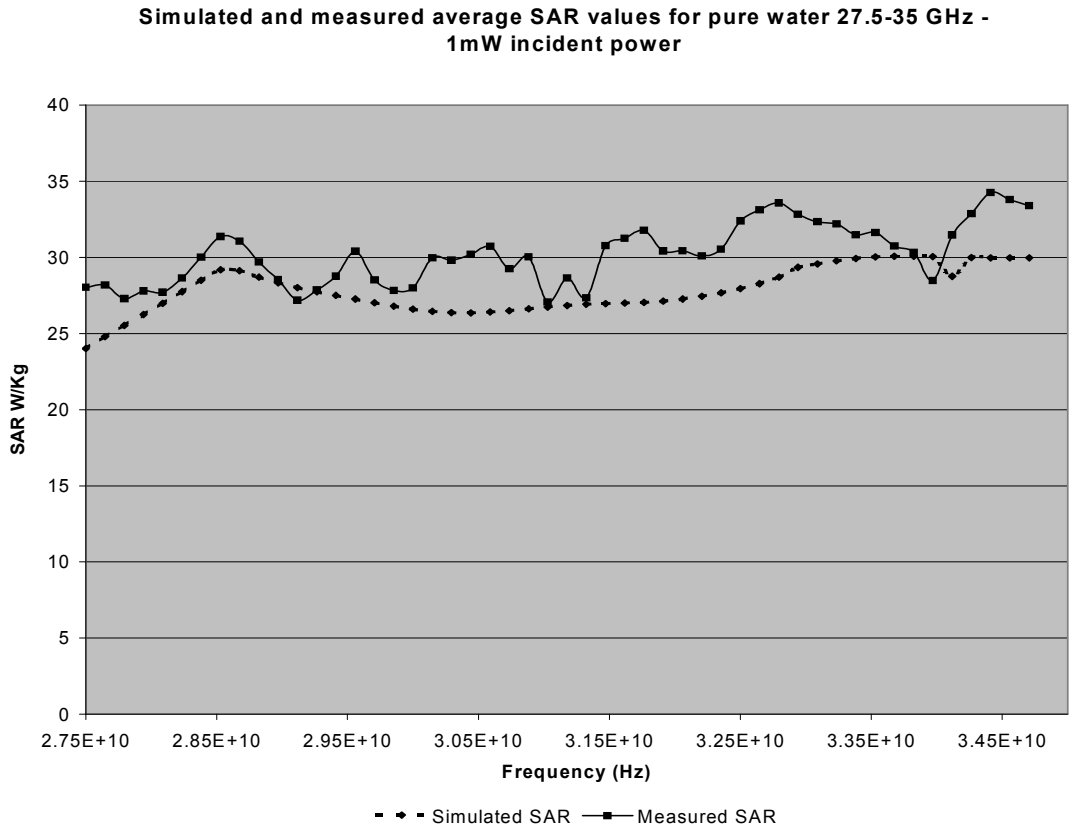

Fig. 23 Simulated and measured SAR with a 1 mW input power

The HFSS model revealed that the isolation between the control detector and the other detectors in the array is in excess of 60 dB. The model takes into account the evanescent modes created within or in the vicinity of the sample. In the event that some ultra-low interaction occurred, which was frequency specific, a corresponding decrease in the calibration sequence threshold would occur.

6.2.4 Power levelling using the frequency doubler / sweeper

The frequency doubler and sweeper combination give a non-linear power output. The power was levelled using an external power meter, used to create a lookup table.

It was also necessary to perform a power flatness calibration. Power measurements were taken from the transmission port of the exposure cell across the operational frequency range. The frequency doubler and sweeper combination give a non-linear power output. The power was levelled using an external power meter that was used to create a lookup table. The absolute levelled maximum output power of the 8510c is –15 dBm. Owing to the absorption characteristics in culture media in the test cell and the small sample volume (approximately 4 µl) specific absorption rates in excess of 1 W can be generated. Higher order harmonics of the frequency source are negligible and the cell is fundamental mode in the 26 – 40 GHz frequency range.

6.3 Performance characteristics of the apparatus

In this section some example runs of the instrument are presented and performance characteristics determined. A significant issue with any detection system is sensitivity. In the system presented here, sensitivity is dependent on the response of the whole cell biosensor to mm-wave radiation and the efficiency of the optics / photodetector and the analysis software.

6.3.1 Preliminary experiments

Preliminary experiments were performed using Photobacterium phosphoreum 844 (NCIMB, Aberdeen, U.K.).and Vibrio fischeri NRRL B-11177 (Agricultural Research Service, IL, USA). The cathode window of the photomultiplier tube was positioned end on to the sample tube. Wide variation in count rate occurred with different runs of the continuous culture system and at different cell densities. On a number of occasions count rates in excess of $1x10^6$ cps were measured which caused the PM tube buffer to overflow. The species Photobacterium phosphoreum was significantly brighter than the other strains studied.

6.3.2 Segmented flow and its measurement using luminometers

The flow segmentation fitting was used as described in chapter 3. Fig. 21 shows the control panel relating to a channel processor. Various windowing parameters appear in dialogue boxes. The left window shows the bubbles going through the system after user defined signal averaging. The irradiated and calibration segments are differentiated by yellow and red trailing menisci. The right channel shows the value of luminosity for the averaged region of each segment and the trend of previous segments. The variations between the luminosity of different segments were accounted for in the analysis of the software.

Fig. 24. Channel processor control panel

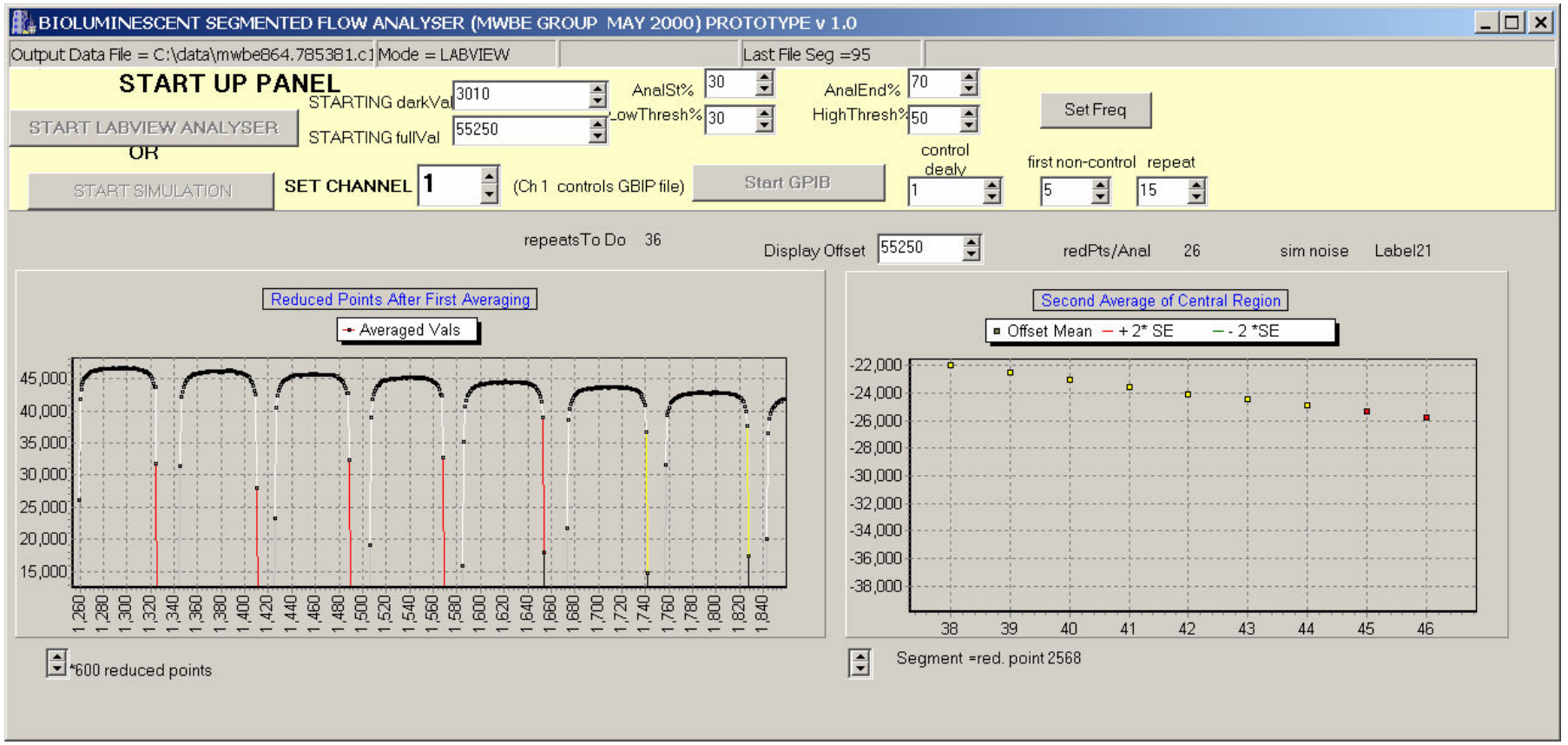

6.3.3 Example spreadsheet

As described in chapter 3, the luminometer data is pre-processed in the channel processor software. Average segment values are used to poll a spreadsheet based comparator program that is illustrated in Fig. 26. Starting with the left column is the segment identification number. The second and third column are the source frequency (GHz) and power in dBm i.e. –110 dBm is considered off and 5 dBm is exposed. Columns C1 and C2 are averaged emission from each segment and C1/C2 is the ratio. See Chapter 3 for details of the methodology. The final three columns relate the statistics of the calibration series, and are used for de-trending the data points.

Seg			C1	C2	C2/C1	C2:CSBM	C2/C1:CP	C2/C1:ST
0	27500000	-110	503.4091	846.4909	1.681517		-0.31433	
1	27500000	-110	495.6818	855.6273	1.726162		2.237834	
2	27500000	-110	518.2222	861.3307	1.662088	1.689939	-1.64808	
3	27500000	-110	425.525	714.9	1.680042		-0.67731	
4	27500000	-110	532.0444	904.4154	1.699887		0.403288	
5	27500000	5	584.1	1051.946	1.800969		6.275765	
6	27510000	5	580.2556	988.1693	1.70299		0.401531	
7	27520000	5	662.0333	1071.617	1.618675		-4.65703	
8	27530000	5	505.77	910.1333	1.7995		5.896631	
9	27540000	5	525.7364	950.8666	1.808638		6.33672	
10	27550000	5	506.3556	843.6539	1.666129		-2.13165	
11	27560000	5	410.6	733.0546	1.785325		4.773903	
12	27570000	5	470.9545	811.06	1.722162		0.974652	
13	27580000	5	533.42	1021.133	1.914314		12.13843	
14	27590000	5	471.0545	828.37	1.758544		2.91953	
15	27590000	-110	568.1636	957.09	1.684532		-1.50194	
16	27590000	-110	417.8364	718.5	1.719573		0.455305	1.008084
17	27590000	-110	451.63	777.8583	1.722335	1.713339	0.525088	-0.40728
18	27590000	-110	410.99	706.2636	1.718445		0.277375	
19	27590000	-110	443.4	763.45	1.721809		0.453008	
20	27600000	5	410.1	716.76	1.747769		1.946586	

Table. 2 Extract from spreadsheet based comparator program

6.4 Operation of the apparatus

6.4.1 Running the apparatus

The growth medium for the organisms was prepared as described in chapter 5, 5 l for the Bioluminostat and 10 l for the mixing tank feed. The entire culturing apparatus and in-line components were autoclaved fully assembled to minimize the possibility of contamination. Cultures were plated to check for contamination at the end of each run.

Refer to chapter 5 for details relating to inoculation and control of the continuous-culture device. When the desired luminosity and cell density were achieved, transfer to the mixing chamber was initiated at 1 ml hr^{-1}. In initial experimentation, the dilution rate of the mixing chamber was adjusted so that a luminous, high-density culture entered the exposure cell. An initial segmentation regime of 1 cm air space – 3 cm sample was used. It should be noted that as the analysis system calculates a windowed average for each segment and so the system is not sensitive to small variations in segment length. The flow rate of the system is measured when steady state conditions have been achieved.

Light emission from the silicone tube was measured with the photomultiplier directed towards the tube and with the collimator fibre optics in place. Count rates in excess of 106 cps (counts per second) could be achieved from cultures of *Photobacterium phosphoreum 844* and this was approximately halved for Vibrio fischeri B-11177. Changes in the source - coupling geometry with the fibre optics and collimator deployed caused a significant decrease in count rate, lowering it to about 103 cps. Background count rates were in the order of 5 cps although some variation existed between tubes.

When steady-state conditions and a good segment profile is achieved the channel processors and comparator program are started as described in the software description. The software can work reliably low count rates, for example 100 cps, although the threshold set for candidate effect

detection (2 standard deviations) will be much larger (typically 1 – 5 % change in intensity through the system). At a count rate of $3x10^3$ cps this was reduced to less than 0.5 %. Measuring the tube directly, it was possible to lower thresholds 0.1 %. Ideally bioluminescence should be sub-maximal so both increases and decreases in bioluminescence can be observed. The species *Photobacterium phosphoreum 844* was observed to clump under certain circumstances and this caused a peak associated with trailing meniscus. The analysis window could be adjusted to exclude this peak that always presented in the same position. Moreover, the addition of a surfactant, Triton X-100 0.1 % (Fisher, U.K.), to the mixing tank reservoir minimized this peak. Temperature was continuously monitored at a number of locations in the analysis area and the variation between sample points determined to vary less than 0.1 ^oC throughout each experimental run. Sample noise in the system had a gaussian distribution.

The comparator program performs an on-line analysis as described in the software section. An example of the output graph is shown in Fig. 22. In this example, the apparatus was programmed to step in 1 MHz increments starting from 25 GHz, a region previously uncharacterised for biological activity. A 1:3 ratio calibration (red) and exposed (yellow) segment regime was employed. In the example, the irradiation time was relatively short at 20 s, a period that was unlikely to induce biological effects. End-on photomultiplier measurements were made to observe the lowest noise conditions possible. Ch 2 corresponded to the syn detector measurements and Ch 3 – 6 were deployed at observation positions 2, 4, 6, 8, min post exposure. Each channel is the ratio between that channel and the pre-exposure detector with the axis as a percent. The yellow points represent irradiated segments; the red segments are non-radiated calibration segments. The blue line is a confidence interval based on the statistics of the calibration sequence. A number of candidate effects are identified. Candidate frequencies (those that fall outside the 95 % confidence threshold) could be re-examined later in the analysis to determine if they represented noise or real effects.

Fig. 25. Output graph from channel comparator software. Yellow squares indicate exposed segments and red squares indicate unexposed calibration segments. The blue line indicates 95 % confidence interval. Note that channel 1 is not shown as it is the pre exposure reference.

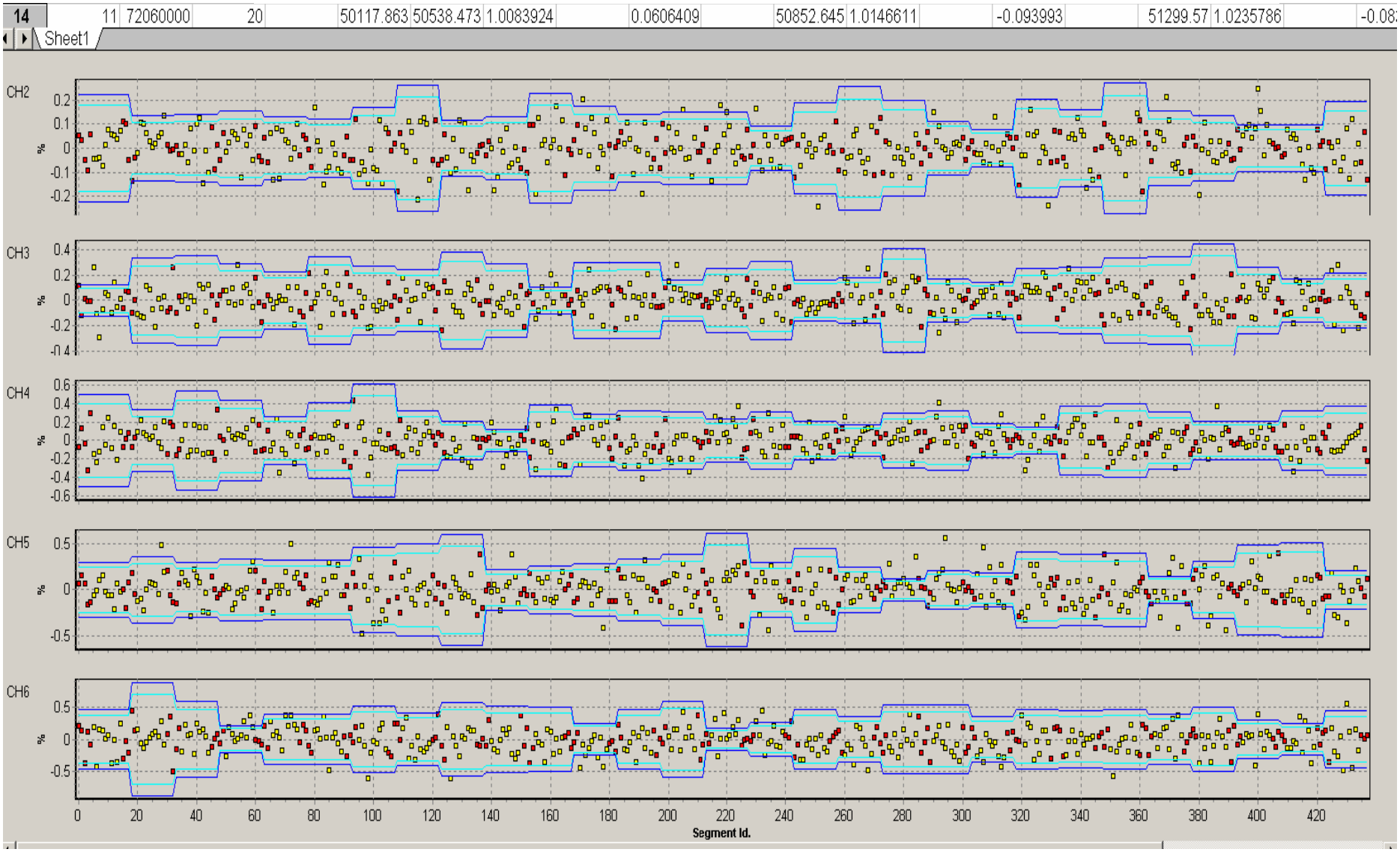

Summary

The performance characteristics of both components and of the entire apparatus are reported. The continuous culture device is used to produce cells suitable for exposure to mm-wave radiation. Its stability and operation over extended periods is demonstrated. Real and simulated data of the exposure cell was compared and showed a close correlation. The channel processor software operation is also shown, it enables the system to track segments and feed information to the comparator software. The comparator software detects relative changes in luminosity pre, syn and post exposure.